# Comparative analysis of electrochemical and spectroscopic sensing of enzymatic reactions: Lactate dehydrogenase-A case study

Microchemical Journal 219 (2025) 115963

Contents lists available at ScienceDirect

Microchemical Journal

journal homepage: www.elsevier.com/locate/microc

# Comparative analysis of electrochemical and spectroscopic sensing of enzymatic reactions: Lactate dehydrogenase-A case study

Chiara Vincenzi [a], Clarissa Cocuzza [a], Andrés Illanes [b], Debora Fino [a], Simelys Hernández [a], Valentina Cauda [a], Carminna Ottone [b,*], Marco Piumetti [a,*]

[a] Department of Applied Science and Technology, Politecnico di Torino, Corso Duca degli Abruzzi, 24, 10129 Turin, Italy
[b] Escuela de Ingeniería Bioquímica, Pontificia Universidad Católica de Valparaíso, Av. Brasil 2085, Valparaíso, Chile

ARTICLE INFO

*Keywords:*
Amperometric biosensor
LDH enzyme
Anticancer drugs
NADH
UV–Vis spectroscopy

ABSTRACT

In this work, electrochemical methods are evaluated as a promising alternative to UV–vis spectroscopy for monitoring Lactate Dehydrogenase (LDH) activity through amperometric detection of NADH, with the aim of screening and assessing the efficacy of potential anticancer drugs. A Ti-modified glassy carbon electrode is used as working electrode, demonstrating effective performance in quantifying NADH. The chronoamperometric measurements conducted at 0.66 V yield a linear response over increasing NADH concentrations. The sensitivity is 0.614 μA $cm^{-2}$ $mM^{-1}$, with a limit of detection (LOD) of 27.58 μM and a limit of quantification (LOQ) of 91.92 μM. The proposed electrochemical set-up shows good selectivity, with no interference-induced signals while maintaining a stable amperometric response upon variations in NADH concentrations. Although the LOD may benefit from further optimization, this electrochemical approach offers some advantages compared to optical methods because it provides higher sensitivity and stability from interference caused by several compounds.

## 1. Introduction

A survey conducted by the International Agency for Research on Cancer (IARC) predicts a significant increase in both new cancer diagnoses and cancer-related deaths over the next 26 years [1], highlighting the need for new therapeutic approaches. Cells from the most prevalent cancer types, including pancreatic, lung, bronchial, colorectal, breast, prostate, and tracheal cancers, adopt altered metabolic pathways to efficiently acquire metabolites and energy [2–11]. Specifically, inhibiting the glycolytic pathway has emerged as a promising strategy to reduce the proliferation of cancer cells [12]. Targeting lactate dehydrogenase (LDH), especially its isoforms LDH-A and LDH-B, appears a strategic approach as LDH is a key enzyme in the deregulated metabolism of cancer cell. It produces lactate, which functions both as an oncometabolite and a signaling molecule, favoring cancer cells proliferation [8,13–15]. Efforts have mainly focused on LDH-A inhibition rather than LDH-B, because LDH-A suppression is unlikely to cause severe side effects, in fact individuals with a complete absence of LDH-A gene only suffers of myoglobinuria after intense exercise [16,17]. Serum LDH levels are frequently elevated in patients with advanced cancers, and high LDH concentrations are correlated with tumor burden and poor prognosis across different malignancies [18–20]. Clinically, LDH is therefore considered a broad metabolic biomarker useful for prognosis and treatment monitoring, but it is not specific enough to serve as an early diagnostic tool [20]. Modern diagnostic technologies, including liquid biopsy and next-generation sequencing, provide much higher specificity and sensitivity for early detection, clearly surpassing LDH in this respect [20–23]. In contrast, LDH, particularly LDH-A, represents an attractive pharmacological target: recent preclinical studies have demonstrated that LDH-A inhibition suppresses tumor growth and enhances chemosensitivity, supporting its relevance for anticancer drug discovery [23–25].

LDH-A catalyzes the reduction of pyruvate to lactate while simultaneously oxidizing the cofactor NADH, as illustrated in Scheme 1.

*Abbreviations:* *h*LDH-A, human lactate dehydrogenase type A; LOD, limit of detection; LOQ, limit of quantification; FDA, food and drug administration; RE, reference electrode; CE, counter electrode; WE, working electrode; GCE, glassy carbon electrode; ID, inner diameter; CV, cyclic voltammetry; LSV, linear sweep voltammetry; EIS, electrochemical impedance spectroscopy; CA, chronoamperometry; IY, immobilization yield; RSD, relative standard deviation; CPE, constant phase element.

* Corresponding authors.
*E-mail addresses:* carminna.ottone@pucv.cl (C. Ottone), marco.piumetti@polito.it (M. Piumetti).

https://doi.org/10.1016/j.microc.2025.115963
Received 30 July 2025; Received in revised form 7 October 2025; Accepted 27 October 2025
Available online 30 October 2025

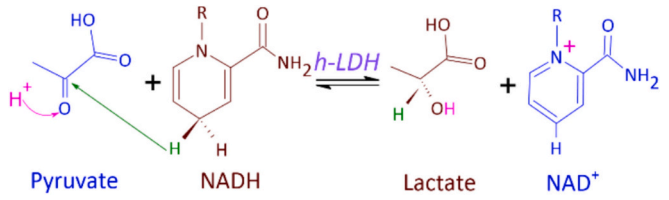


**Scheme 1.** Schematic representation of the enzymatic reaction catalyzed by human Lactate Dehydrogenase (*h*LDH), showing the conversion of pyruvate to lactate coupled with the simultaneous oxidation of NADH to $NAD^+$.

According to Food and drug administration (FDA), the development for new drugs to be approved and commercialized is a time-demanding and expensive process [26]. Drug development typically requires an average of 12 years and around USD 2.7 billion for each new drug [27,28].

In this context, the development of a device which can be used to test different compounds for assessing enzyme activity in the presence of candidate inhibitors, could accelerate the new drugs screening phase and reduce the associated costs [29,30]. The proposed device could consist of two different sections: the first, containing the confined enzyme, is responsible for the enzymatic reaction, while the purpose of the second section is to measure the enzymatic activity. Enzymatic activity can be monitored using different techniques. Among them, the optical and electrochemical approaches enable real-time follow-up of the enzymatic reaction [31–33]. The separation of the biorecognition component from the transducer seems a promising approach to overcome the issues related to the short lifetime of the enzymes and the non-conductivity of enzyme carriers in case an electrochemical approach is selected [31,34–38]. Strategies combining enzymes with nanozymes or metal–organic frameworks have been shown to improve the stability and efficiency of bioelectrochemical systems [31,32].

Moreover, covalent immobilization of enzyme on mesoporous silica is extensively used and investigated to recover the biocatalyst and prevent the leakage of the enzyme that would affect the storage and the working stability of the biorecognition component [31,39–45].

The objective of this study is evaluating the electrochemical approach as a possible alternative to UV–vis spectroscopy for monitoring the enzymatic activity of *h*LDH-A, specifically aimed at screening anticancer drugs formulated as lactate dehydrogenase inhibitors. Several NADH detection strategies have been developed, including fluorescence-based assays and microfluidic platforms. Fluorescence methods offer high sensitivity and selectivity but typically require labeled reagents and sophisticated optical instrumentation, which can limit scalability and increase costs [46,47]. Microfluidic systems provide advantages in miniaturization and process integration; however, the detection component is generally modular and must be specifically tailored to the analyte and experimental conditions [48,49]. In contrast, the electrochemical sensing approach appears as a suitable solution offering high specificity and selectivity while allowing real-time measurements, with label-free quantification of NADH, relatively simple instrumentation and cost-effectiveness [31–33,35,50,51]. Since the concentration of NADH is directly correlated with enzymatic activity, accurately measuring NADH levels enables real-time monitoring of the *h*LDH-A catalyzed reaction and consequently the estimation of enzyme activity [52–55].

In this study, the UV–Vis spectroscopy and electrochemical approach are both used to measure NADH concentration and, consequently, to monitor lactate dehydrogenase activity both with and without inhibitors. The optical measurements are carried in a UV–Vis spectrophotometer set at NADH absorption peak (340 nm), while the electrochemical analyses are performed with a conventional three-electrode set-up equipped with a Ti modified glassy carbon electrode (GCE) as working electrode. The electrochemical characteristics of the set-up were investigated with voltammetry, impedance spectroscopy and chronoamperometry techniques.

## 2. Materials and methods

### 2.1. Materials

Titanium microparticles (<45 μm), 1,2,3-trimethylbenzene (TMB or mesitylene), Pluronic P-123, tetraethyl orthosilicate (TEOS), (3-glycidyloxypropyl)trimethoxysilane (GPTMS), (3-Aminopropyl)triethoxysilane (APTES), sulfuric acid, hydrochloric acid (37 % wt.), ethanol, acetone, $CuSO_4$, $KH_2PO_4$, $K_2HPO_4$, $NaHCO_3$, $Na_2CO_3$, 1-hydroxy-6-phenyl-4-(trifluoromethyl)-1H-indole-2-carboxylic acid methyl ester (NHI-2), dimethylsulfoxide (DMSO), and L-lactate dehydrogenase from human (*h*LDH-A, EC 1.1.1.27) expressed in *Escherichia. coli* were supplied by Sigma-Aldrich (Merck). Potassium iodide, sodium meta periodate, lactic acid, sodium pyruvate, sodium borohydride, Galloflavin, and NADH were purchased from VWR Avantor. 10 wt% Nafion water-based solution was purchased by Fuel Cell Earth.

### 2.2. Enzyme support

#### 2.2.1. Mesoporous silica synthesis, functionalization and characterization

The mesoporous silica support was synthesized through the hydrothermal synthesis method and functionalized to provide amino and aldehydic functional groups, as described by our previous work [56]. For the sake of clarity, the procedure is briefly described in the Supporting Information.

As previously reported, the resulting glyoxyl groups formed on the silica surface were quantified through the back-titration method with $NaHCO_3$/KI, while the amino groups were quantified by the interaction between $CuSO_4$ and -$NH_2$ groups [56–58].

The synthesized support was characterized in terms of morphology and structure by high-resolution field emission scanning electron microscopy (FE-SEM) and high-resolution transmission electron microscopy (HR-TEM). Surface chemical properties were investigated through Fourier transform IR (FT-IR), while ζ-potential analysis was performed to evaluate the surface charge. Textural features were evaluated through $N_2$ physisorption at 77 K. Detailed procedures are provided in the Supporting Information.

### 2.3. Biocatalyst

#### 2.3.1. Lactate dehydrogenase features

The enzyme analyzed in this research is the human lactate dehydrogenase expressed in *Escherichia coli* (UniProt ID. K1T0A2) hereafter referred to as *h*LDH-A. Its minimum diameter can be estimated by applying Eq. (1) [59].

$$D_{min} = 2 \bullet \left(0.066 \bullet \sqrt[3]{M}\right) \quad (1)$$

where $D_{min}$ is the minimum diameter of the enzyme whose shape is approximated to a sphere (nm) while M is the molecular weight of the enzyme (Da), equal to 27.46 kDa for *h*LDH-A, according to UniProt database. Consequently, its minimum diameter is 3.98 nm.

#### 2.3.2. UV spectroscopic response

The enzymatic performances were evaluated at 35 °C and pH 7.5 using an UV–vis spectroscopy with a Jasco V-730 instrument. The measurements were carried out at 340 nm, the wavelength corresponding to the absorption peak of NADH. A solution of 2.9 ml containing 0.24 mM NADH and 1.69 mM pyruvate in 0.1 M phosphate buffer pH 7.5 was used as a blank. Then, 100 μl of *h*LDH-A solution (0.01 mg $ml^{-1}$) were added to the blank solution. The specific activity of *h*LDH-A ($A_{FE}$, U $mg^{-1}_{prot}$) was 379.1 ± 6.0 U $mg^{-1}_{prot}$, calculated using Eq. (2).

$$A_{FE} = \frac{\Delta A}{\varepsilon L} \cdot \frac{V_s}{V_e} \cdot \frac{1}{c_e} \quad (2)$$

where ΔA is the absorbance slope, ε is the NADH molar extinction coefficient (6.22 $mM^{-1}$ $cm^{-1}$), L is the optical path (1 cm), $V_s$ is the volume of the solution in the cuvette (ml), $V_e$ is the volume of enzymatic solution (ml), and $c_e$ is the concentration of the enzymatic solution (mg $ml^{-1}$). The specific activity of the immobilized *h*LDH-A ($A_{IE}$, U $g_{supp}^{-1}$) was calculated using Eq. (2) as well, where $V_e$ (0.1 ml) and $c_e$ (0.02 g $ml^{-1}$) represent the volume and the concentration of the immobilized enzyme suspension, respectively.

### 2.3.3. Enzyme immobilization

The enzyme was immobilized on the functionalized support, adapting the multipoint covalent method reported in our previous work. [56]. For clarity, the procedure is briefly summarized in the Supporting Information. The immobilized enzyme hereafter is referred to as Biocat.

FT-IR spectra were acquired on Biocat, and on the functionalized support to highlight the differences due to the covalent bonds formed between the enzyme and the support. The IR spectra were acquired using a Bruker INVENIO instrument equipped with a liquid nitrogen cooled MCT detector. The samples were degassed to $10^{-3}$ mbar and the analyses were performed at room temperature (range 4000–400 $cm^{-1}$, 64 scans, resolution 4 $cm^{-1}$).

Optical fluorescence microscopy was conducted to analyze the presence and distribution of the enzyme on the support by observing the labeled enzyme immobilized on mesoporous silica. The procedure previously described by Rocha-Martín et al. was used to label the enzyme [60]. The same procedure was described in our previous work [56], for the sake of clarity it is reported in the Supporting Information.

### 2.3.4. Activity tests in the presence of inhibitors

Kinetic tests were performed on Biocat both with and without inhibitors NHI-2 and Galloflavin, as described in section 2.4 The concentration of pyruvate was varied in the range 5–200 μM as indicated. These tests were repeated with the addition of 20 μl of 3.02 mM NHI-2 solution or 20 μl of 824.46 μM Galloflavin solution. Since both inhibitors were diluted in dimethyl sulfoxide (DMSO), the activity of the biocatalyst was also studied in the presence of DMSO. The results obtained with Biocat were compared to those obtained under the same conditions with free *h*LDH-A. Each data point was measured in triplicate, and the apparent kinetic parameters were determined according to the Lineweaver-Burk linearization method.

### 2.3.5. Enzyme molecular modeling

Molecular modeling simulations were performed to investigate the interactions between NHI-2 and Galloflavin and the enzyme. Computational analyses were carried out for each ligand individually, using Vina AutoDock. Subsequently, ligands were docked in their minimum energy conformation, and exploratory structure analysis was implemented to identify hydrogen bonds between the ligand and enzyme's amino acid residues. The molecular structures of ligands were obtained from PubChem, while the enzyme molecular structure was obtained from the Uniprot data bank (UniProt ID. K1T0A2) [61].

### 2.3.6. Optical analysis of reagents and interferents in enzymatic reactions

The optical absorption spectra (255–745 nm) of the substrate (pyruvate), cofactor (NADH), and products (lactate and $NAD^+$), along with the inhibitors (NHI-2 and galloflavin) and their solvent (DMSO), were recorded using a Jasco V-730 UV–vis spectrophotometer.

## 2.4. Electrochemical setup and measurements

Electrochemical measurements were implemented using Palmsens4 as a potentiostat, in a conventional three-electrode configuration. Ag|AgCl, 3 M KCl was used as the reference electrode (RE), a Pt wire served as the counter electrode (CE), and Ti-modified glassy carbon electrode (GCE, ID =3 mm) as the working electrode (WE). The GCE was employed due to its widespread application in NADH detection [55,62–64]. Ti microparticles, acting as redox-active mediators, were deposited on the GCE surface to lower the overpotential required for NADH oxidation, improving measurements accuracy and avoiding high-potential side reactions, such as hydrogen evolution, radical formation, or dimerization, that can reduce selectivity and compromise the reliability of the electrochemical signal [65–67]. A total of 10 layers of Ti suspension (10 mg $ml^{-1}$ in ethanol) were drop-cast on the surface of GCE, resulting in a final amount of 0.2 mg of Ti. Subsequently, Nafion (5 μl, 10 wt%) was used as a binder to immobilize Ti on the GCE surface [68–71]. The current density reported in the graphs was obtained by normalizing the measured current to the geometric area of the working electrode (0.0707 $cm^2$).

Each electrochemical test was conducted at room temperature in 0.1 M phosphate buffer (pH 7.5). Before each test, the system was pretreated by bubbling nitrogen at a flow rate of 30 ml $min^{-1}$ for 30 min and, subsequently, performing 3 cycles of cyclic voltammetry, within a potential range of 0 to 1 V with a scan rate of 20 mV $s^{-1}$. **Fig. S1** in the Supporting Information (SI) illustrates the electrochemical setup used.

*Cyclic voltammetries (*CVs) were performed within the potential range of 0 and 1 V with a scan rate of 20 mV $s^{-1}$ in the presence of 5 mM NADH. CVs were performed both with bare and modified GCE to better highlight Titanium microparticles role.

*Linear sweep voltammetries* (LSVs) were performed in the range between 0 and 1 V. The scan rate varied from 1 to 100 mV $s^{-1}$ and the NADH concentration varied from 0.7 to 5 mM, as indicated.

*Electrochemical impedance spectroscopy (EIS)* was performed by setting the DC potential ($E_{DC}$) at 0.66 V and the AC potential ($E_{AC}$) at 0.01 V, while varying the frequency from $10^5$ to $10^{-2}$ Hz.

*Chronoamperometry (CA)* response was studied at 0.66 V. The current signal was stabilized before starting the analysis. After each addition of NADH or interferents to reach the appropriate concentration, the solution was vigorously stirred for 10 s, then the stirring was turned off and the signal was recorded for 180 s. Throughout the analysis, nitrogen was bubbled in the system at a flow rate of 30 ml $min^{-1}$.

## 2.5. Electrochemical response of the biocatalyst

To evaluate the suitability of the proposed electrochemical apparatus for studying enzymatic activity, the amperometric response of 0.23 mM NADH and 1.63 mM pyruvate in 0.1 M phosphate buffer pH 7.5 solution was monitored at room temperature using chronoamperometry at 0.66 V. The chronoamperometric test was performed as previously described in section 2.4 and the current signal was stabilized before adding the enzyme (0.01 mg of free *h*LDH-A or 20 mg of Biocat). The test was repeated in the presence of inhibitors at the same concentrations specified in Section 2.3.4.

# 3. Results and discussion

## 3.1. Mesoporous silica characterization

**Fig S2. Section a** and **b** in the Supporting Information reports FE-SEM and HR-TEM images of the mesoporous silica support. The support displays rounded formations ranging from 0.7 to 1.9 μm. Moreover, the material exhibits bent channels oriented in perpendicular and longitudinal directions; this is likely due to the high swelling/directing (TMB/P-123) agents ratio used to synthetize this mesoporous silica [56,72–74].

The subsequent functionalization step introduced about 1.01 mmol $g^{-1}$ of glyoxyl groups and 1.30 mmol $g^{-1}$ of amino groups onto the support surface. The ζ-potential of the functionalized silica dispersed in a 25 mM carbonate buffer (pH 9) containing 300 mM trehalose was measured to be −16.8 ± 3.3 mV. The negative value of the ζ-potential

was previously ascribed to the deprotonation of silanols groups [75,76]. The functionalization process reduces the cumulative pore volume from 0.6 $cm^3\ g^{-1}$ to 0.3 $cm^3\ g^{-1}$, with a consistent reduction of pore diameter from 4.2 nm to 3.8 nm, probably due to the complete or partial occlusion of the smallest pores by APTES and GPTMS [77,78]. Similarly, the specific surface area is reduced from 673 $m^2\ g^{-1}$ to 301 $m^2\ g^{-1}$. However, in both cases, the samples exhibited type IVa isotherms with H2b hysteresis loop according to IUPAC classification [56,79,80]. **Fig. S3** of the Supporting Information displays the $N_2$ physisorption isotherms and pore size distribution ($dV/dD_{pore}$) collected on the support before and after the functionalization.

The comparison of the FTIR spectra acquired on the pristine and functionalized support (**Fig. S4** in the SI) confirms the surface modification resulting from the functionalization process. Evidence of successful functionalization is observed in the 2200–1340 $cm^{-1}$ region, where new absorption bands appear, corresponding to the characteristic vibrational modes of -CO and -NH groups. In the 4000–2500 $cm^{-1}$ region, chemical modifications on the silica surface are evidenced by absorption peaks around 2900 $cm^{-1}$ and 3400 $cm^{-1}$, corresponding to $-CH_2$ vibrations and hydrogen-bond interactions, respectively. Moreover, the absorption signals associated with surface silanols are either absent or significantly reduced in the functionalized sample, indicating the involvement of these groups in forming bonds with organosilane molecules. **Table S2** in the SI reports a comprehensive list of the identified absorption peaks [56,58].

### 3.2. Enzyme immobilization

*h*LDH-A was covalently attached to the functionalized silica support as detailed in the SI. The immobilization yield (IY) of the enzyme on the support was 86 %, resulting in a specific activity of the immobilized enzyme ($A_{IE}$) of 123 U $g_{supp}^{-1}$. This corresponds to a retained activity ($R_{act}$) of 34.7 %.

**Fig. S5** in the SI depicts the images acquired through fluorescence microscopy of the enzyme immobilized on functionalized mesoporous silica. The presence of *h*LDH-A is confirmed by distinct red spots visible in **Fig. S5 (Sections a and b)**. Notably, red spots overlap blue (**Section c**) and green fluorescence signals (**Section d**). Since the blue and green spots are the results of the intrinsic emission of the functionalized silica (as highlighted by **Fig. S6, SI)**, the analysis confirms the presence of the enzyme on the support as a consequence of the immobilization [56,58].

Further insights into the nature of enzyme-support interactions were obtained by comparing the FTIR spectrum acquired on Biocat with that of the functionalized silica. As shown in Fig. 1, the absorption peak at ca. 1600 $cm^{-1}$ (pink area) in the immobilized enzyme spectra is readily attributed to the stretching signal of amide I (R-C(=O)-NR'R") [56,81].

On the other hand, the signals at 1711 $cm^{-1}$ and 1723 $cm^{-1}$ (yellow area) are ascribed to $-CH_2$-C(=O)- and -C=O stretching respectively [82,83], whereas the band at 1530 $cm^{-1}$ corresponds to -Si-$NH_2$ vibration modes. The reduced intensity of the latter peaks suggests the involvement of both -C=O and -$NH_2$ groups in the bond formation between the LDH and the solid support. These findings are consistent with the multipoint covalent immobilization technique [84].

### 3.3. Evaluation of biocatalyst performance

Since the proposed device aims to evaluate the effect of inhibitors (e.g., NHI-2 and Galloflavin) on *h*LDH-A, kinetic analyses were performed on both free and immobilized enzyme. **Fig. S7** (SI) shows the obtained results, fitted using the Lineweaver–Burk linearization method. The kinetic behavior of free *h*LDH-A (**Section a**) remains consistent regardless of the presence or absence of DMSO. An F-test comparing the two linear models revealed no statistically significant differences. Conversely, DMSO appears to exhibit inhibitory behavior for immobilized *h*LDH-A (**Section b**). This effect may be due to conformational changes in the enzyme structure caused by immobilization, which could enhance

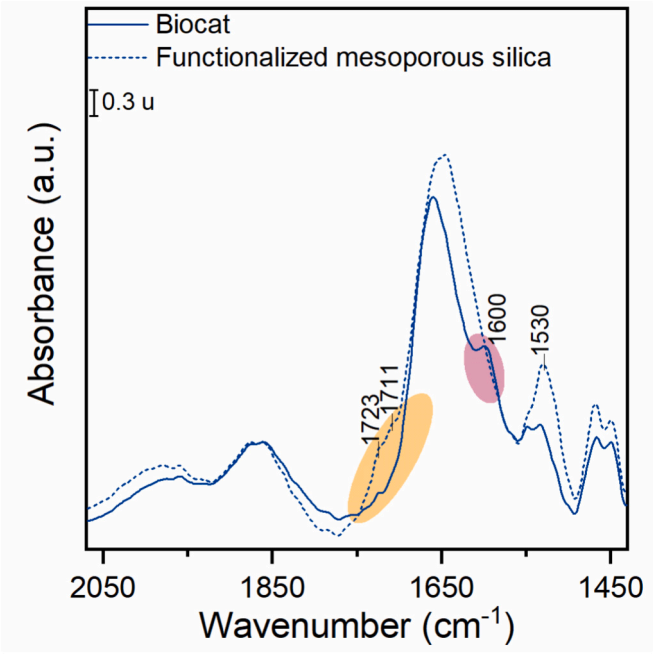


**Fig. 1.** FT-IR spectra of the immobilized enzyme Biocat and the functionalized support (region 2070–1430 $cm^{-1}$) collected in vacuum conditions at room temperature.

secondary interactions between the enzyme and DMSO, ultimately reducing enzymatic activity. The apparent kinetic parameters, $V_{max}$, the maximum achievable rate, and $K_M$, the Michaelis-Menten constant which indicates the enzyme's affinity for the substrate, can be determined by applying the Lineweaver-Burk model to activity data obtained at varying substrate concentrations. **Table S3** (SI) lists the apparent values obtained. The values of $V_{max}$ and $K_M$ obtained with NHI-2 and Galloflavin are likely to describe a mixed-type inhibition. The mixed-type inhibition is typically caused by allosteric effect. These inhibitors may determine conformational changes of the three-dimensional structure causing the obstruction of enzyme activity [85]. Mixed-type inhibition may have a positive or negative modulation depending on the values of the apparent kinetic parameters [86]. To better understand the interaction mechanism underlying this inhibition, a molecular docking analysis was conducted. **Fig. S8** depicts the crystal poses of *h*LDH-A, in complex with pyruvate and NADH, interacting with NHI-2 and Galloflavin, respectively. In accordance with what was previously reported, both NHI-2 and Galloflavin present their minimum energy configuration when they occupy an allosteric site separated from the active site. The analysis of the interaction between NHI-2 and *h*LDH-A does not highlight any hydrogen bond suggesting the presence of weaker secondary interactions. By contrast, Galloflavin forms two hydrogen bonds with ILE 47 and VAL 48 residues.

To ensure reliable use of the immobilized enzyme, its stability during storage and repeated assays was evaluated. To evaluate the operational lifetime, four consecutive UV–Vis assays were carried out using the same batch of immobilized LDH. After each assay, the biocatalyst was recovered by centrifugation at 1000 rpm for 5 min, washed, redispersed in phosphate buffer, and reused. Each measurement lasted 600 s, and the enzyme activity was determined from the initial slope of absorbance at 340 nm over the first 60 s. The results, shown in **Fig. S9**, indicate negligible variations among the individual runs. The relative standard deviation of the enzymatic activity across the four cycles was only 6 %, demonstrating that the immobilized enzyme can be reliably reused for at least four consecutive assays without significant loss of activity.

The storage stability of the immobilized enzyme was also investigated. After immobilization, the biocatalyst was stored in 0.1 M

phosphate buffer (pH 7.5) at 4 °C and periodically tested by UV–Vis. **Fig. S10** reports the residual activity, expressed as the ratio between the activity at the sampling time and the initial activity immediately after immobilization. After one week of storage, the enzyme retained approximately 40 % of its initial activity, indicating a moderate but acceptable shelf life for the intended screening applications.

To experimentally verify the suitability of UV–Vis spectroscopic monitoring for evaluating inhibitors' effect on enzyme activity, the absorption spectra of individual reaction components were analyzed (**Fig. S11**). As observed, pyruvate exhibits negligible absorption at both 260 nm and 340 nm, while lactate displays a peak at 280 nm, which is largely masked by the overlapping signals of $NAD^+$ and NADH. NADH is characterized by a strong absorption peak at 260 nm, where $NAD^+$ also absorbs, and a distinct peak at 340 nm, at which $NAD^+$ shows no detectable absorption. As a result, the enzymatic reaction is commonly monitored by measuring the absorbance at 340 nm, generated by NADH consumption which is stoichiometrically equivalent to pyruvate consumption with the concomitant production of lactate and $NAD^+$. This method relies on the assumption that no reagents or products interfere with absorbance variation at this wavelength.

However, while the solvent (DMSO) exhibits no significant absorption within the analyzed spectral range, both galloflavin and NHI-2 display notable absorption features. Galloflavin shows a minor peak at 400 nm, with a broad absorption band extending between 255 and 430 nm, whereas NHI-2 presents two distinct absorption peaks, one at 260 nm and another at 330 nm. Although galloflavin exhibits only moderate absorbance at 340 nm, NHI-2 displays a significant absorption peak at this wavelength, potentially interfering with the accurate monitoring of NADH consumption. This spectral overlap raises concerns regarding the reliability of UV–Vis spectroscopy as an optimal method for tracking reaction kinetics and assessing inhibitory effects. Therefore, alternative analytical techniques, such as electrochemical measurements, may be required to ensure precise quantification of enzymatic activity and inhibitor efficacy.

### 3.4. Electrochemical response

Fig. 2 shows the CV curves obtained with Ti-modified GCE over 30 cycles and the LSV curves obtained at increasing NADH concentration. As shown in Fig. 2 **section a**, the system demonstrated high stability, with a relative standard deviation (RSD) of 1.27 % at the NADH oxidation peak. The insert of Fig. 2 **section a** depicts the CV cycles obtained with and without 5 mM NADH. As can be seen, no oxidation peak around 0.69 V was detected when the measure was performed without NADH. The oxidation peak observed with the titanium-modified electrode is lower than that obtained with an unmodified GCE, as demonstrated in **Fig. S12** of the supporting information, which compares the CVs from both modified and unmodified electrodes. This figure clearly shows that the current in the absence of titanium is significantly higher, and the oxidation peak is more defined, albeit occurring at higher potentials. The reduction in potential is one of the primary reasons for modifying the working electrode with redox mediators.

Moreover, the CV curves of the repeatability analysis performed over 6 consecutive tests are shown in **Fig. S13** (SI). The RSD at the NADH oxidation peak is 7.65 %. This result suggests an acceptable repeatability of the modified electrode for NADH detection. The inter-electrode reproducibility of the Ti-modified GCEs was evaluated as well by comparing the anodic peak currents recorded on six independently prepared electrodes under identical experimental conditions. An inter-electrode RSD of 18.9 % was obtained, which reflects the intrinsic variability introduced by the manual multi-layer drop-casting procedure and slight heterogeneities in the modified layer. Although this value indicates that the reproducibility between electrodes is not optimal, it is fully consistent with what is typically observed for enzyme-based electrochemical sensors, including screen-printed platforms, where inter-electrode RSD values in the 10–20 % range are commonly reported due to fabrication-related variability [87–90]. Importantly, despite this level of dispersion, the system consistently provided reliable analytical responses, demonstrating good sensitivity and stable electrochemical behavior. This confirms that the sensor design is robust and functional even in the presence of moderate variability between electrodes.

**Fig. S14** illustrates cyclic CVs acquired using a bare GCE as the working electrode. It is evident that, despite yielding a higher current density, the unmodified electrode exhibited poor signal stability across successive CV cycles. Specifically, the signal was characterized by significant noise and inconsistent overlap between consecutive cycles. This lack of reproducibility strongly suggests that the absence of a redox-active mediator leads to unreliable measurements, likely attributable to the formation and subsequent adsorption of side products on the GCE surface [91].

LSV profiles were recorded at NADH concentrations comprised between 0.7 mM and 5 mM with a potential scan rate of 20 mV $s^{-1}$ (Fig. 2, **Section b**). As can be easily noticed, the anodic current density increased with the increase of the NADH concentration.

As a result of the LSV at different concentrations, the potential value

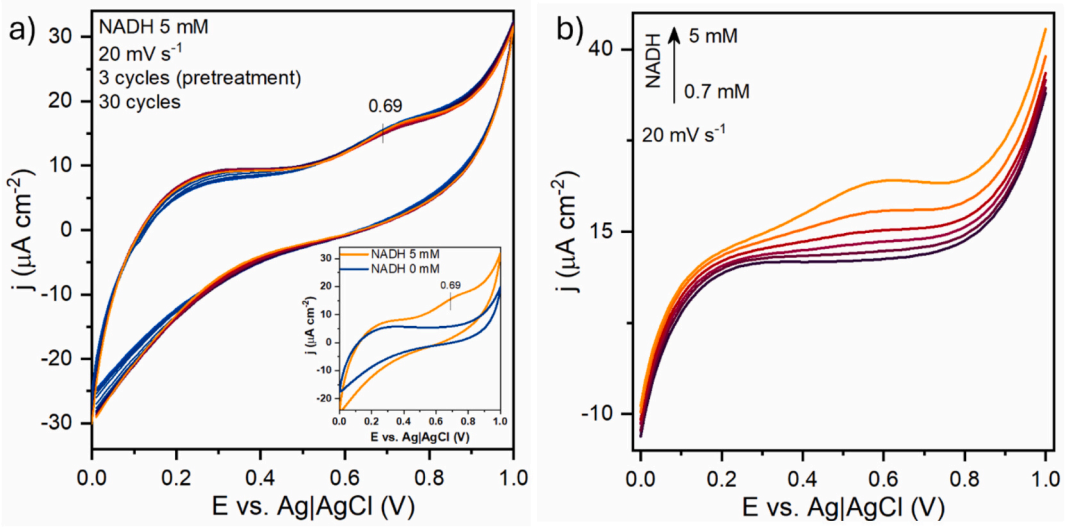


**Fig. 2.** (a) Cyclic voltammograms of Ti-modified GCE in blank and 5 mM NADH solutions and (b) linear sweep voltametric response for NADH concentration comprised in the range 0.7–5 mM recorded with a potential scan rate of 20 mV $s^{-1}$.

of 0.66 V was selected for performing chronoamperometric and EIS measurements. EIS measurements were carried out to obtain insights concerning the charge transport mechanisms across the electrode-electrolyte interface [92]. The impedance spectra were analyzed in Nyquist representation (**Fig. S15**, Supporting information) and fitted using equivalent circuits that account for $R_u$, which is the uncompensated resistance of the electrolyte, determined by the distance between the WE and RE; $R_{ct}$, which corresponds to the charge transfer resistance of the electrochemical reaction, assuming that the redox species are not adsorbed on the electrode surface [31]; $Z_W$ (Warburg impedance), which expresses the mass transport limitations of the redox species to the electrode surface, based on a model of semi-infinite linear diffusion and the constant phase element (CPE), used in place of an ideal capacitor to model the charging and discharging of the electric double layer, accounting for the behavior of real graphite electrodes [93]. Comparative EIS measurements were performed under four conditions: bare and Ti-modified GCE in pure phosphate buffer, and the same two electrodes in the presence of 5 mM NADH (**Fig. S15**). In pure buffer, both electrodes exhibit very large charge transfer resistances (**Fig. S15 section a**), as evidenced by the absence of a closed semicircle in the Nyquist plots. This behavior is expected since, under these conditions, no faradaic reactions take place at 0.66 V. Consequently, the electrode/electrolyte interface behaves as a blocking interface dominated by interfacial capacitance and solution resistance, leading to very large semicircles that do not close within the frequency range investigated [94,95]. The equivalent circuit used to fit these data consisted of an R–W branch in parallel with a CPE, yielding charge transfer resistances of 3.4 $\times 10^4$ Ω for the bare GCE and 1.07 $\times 10^6$ Ω for the Ti-modified GCE. The higher resistance for the latter is attributed to the Nafion overlayer used as a binder, which acts as an additional barrier to charge transport and, in turn, to charge transfer, by hindering ionic conduction and slowing the diffusion of electroactive species [96,97]. In the presence of NADH, the impedance spectrum of the bare GCE (**Fig. S15 section b**) was well fitted by a classical Randles-type equivalent circuit, indicating fast direct NADH oxidation (Rct ≈ 4.6 $\times 10^3$ Ω), consistent with literature reports for glassy carbon electrodes [98]. In contrast, the Ti-modified electrode (**Fig. S15 section c**) required a two-branch equivalent circuit (R–ZW in series, in parallel with CPE), reflecting the coexistence of charge transfer and diffusional processes that cannot be captured by a simple Randles model [94]. The Ti-modified electrode displayed a substantially higher Rct (≈ 8.7 $\times 10^4$ Ω), indicative of slower interfacial kinetics for NADH oxidation. This effect is actually beneficial for the sensing strategy: by slowing the direct electrochemical oxidation of NADH, the Ti/Nafion modification minimizes competition between the electrode and the LDH-catalyzed enzymatic reaction, ensuring that NADH is primarily consumed by the enzymatic pathway. This prevents uncontrolled electrochemical NADH oxidation and improves the reliability of enzymatic activity readouts [99]. This confirms also that, although the potential required for NADH oxidation is relatively high, with the possibility of electrode fouling, the combined use of Ti microparticles and a Nafion overlayer changes the dominant interfacial process, stabilizing and structuring the electrode/electrolyte interface during oxidation and mitigating also surface fouling. In particular, the clear separation between charge-transfer and diffusional contributions in the impedance response is consistent with the sustained electrocatalytic activity observed over multiple measurements, supporting the robustness of the sensing interface during NADH detection.

Fig. 3 (**Section a**) shows the voltammetric response at the increase of the potential scan rate, which can give insights concerning the rate determining step of the electrochemical oxidative process. LSVs were considered to perform kinetic evaluation of the electrochemical system, instead of CV, since no reduction peak was observed in the previous shown CV (Fig. 2 **section a**). As it can be observed from Fig. 3 (**Section b**), the increase of potential scan rate caused a displacement of the oxidation peak toward higher potential. This result, together with the outcomes of the EIS measurements, would support that NADH oxidation is an irreversible process [100]. Importantly, the irreversibility of the NADH oxidation is further supported by the absence of a corresponding reduction peak in the cathodic scan, as can be seen from Fig. 2 **section b**. According to established electrochemical criteria [100], the difference between anodic and cathodic peak potential is a key indicator of the reversibility of an electron transfer reaction. In this case, the lack of a cathodic peak within the examined potential window suggests that the reduction process occurs at much more negative potentials, thus the difference between oxidation and reduction potential being higher than 200/n mV, where n represents the number of electrons involved in the redox process, confirming the irreversibility of the oxidation process under the experimental conditions. In addition, the linear proportionality between the peak current and the square root of the potential scan rate (Section c) suggests a diffusion-controlled behavior [101].

For irreversible processes, the current is limited by the rate of charge transfer. The peak current is related to the rate constant by Eq. (3).

$$\ln(i_p) = \ln(0.227 \bullet A \bullet F \bullet k^0 \bullet C_0) + \left(\frac{\alpha \bullet F}{R \bullet T}\right)(E_p - E^{0'}) \quad (3)$$

where $i_p$ is the peak current, A is the geometrical area of the WE, F is the Faraday constant, $k^0$ is the standard rate constant, $C_0$ is the bulk concentration (5 $\bullet 10^{-6}$ mol $cm^{-3}$), α is the charge transfer coefficient, R is the gas constant, T is the temperature, $E_p$ is the anodic peak potential, and $E^{0'}$ is the formal standard potential (usually known). The values of α and $k^0$ can be derived from the slope and the intercept of the linear plot of $\ln(i_p)$ vs. $E_p$-$E^{0'}$ (**Section d**), respectively.

The value of α is 0.362 while the value of $k^0$ is 5.5 $\bullet 10^{-6}$ cm $s^{-1}$, in agreement with the low values (<$10^{-5}$ cm $s^{-1}$) typical of irreversible systems [100]. In the case of irreversible systems, the diffusion constant can be derived from the slope of $i_p$ vs. $\nu^{1/2}$ plot (**Section c**) because the modified Randles-Ševčík Eq. (4) can be applied [100,102].

$$i_p = 2.99 \bullet 10^5 \bullet n^{3/2} \bullet \alpha^{1/2} \bullet A \bullet C^0 \bullet \mathscr{D}^{1/2} \bullet \nu^{1/2} \quad (4)$$

where $\mathscr{D}$ is the diffusion constant, n is the number of electrons, $\nu$ is the potential scan rate. The other terms have been previously defined. Indeed, the diffusion constant resulted to be 3.22 $\bullet 10^{-9}$ $cm^2$ $s^{-1}$.

Chronoamperometric measurements were performed to determine the sensitivity and selectivity of the electrochemical apparatus as a NADH sensor (Fig 3**. Sections e** and **f**, respectively).

Before starting with the NADH addition, a quasi-stationary current density of 0.2104 μA $cm^{-2}$ with a standard deviation (σ) of 5 $\bullet 10^{-3}$ μA $cm^{-2}$ was achieved. The amperometric response was linear over the entire range tested (0.05–2 mM NADH), the sensitivity (S), calculated as the slope of the calibration curve, was 0.614 μA $cm^{-2}$ $mM^{-1}$, the LOD was 27.58 μM and the LOQ was 91.92 μM. The LOD and LOQ were calculated by applying Eq. (5) [55,69,71,103].

$$\text{LOD or LOQ} = k \bullet \frac{\sigma}{S} \quad (5)$$

where k is equal to 3 for LOD and equal to 10 for LOQ, σ is the standard deviation of the blank, and S is the sensitivity of the calibration curve.

The selectivity of the proposed electrochemical apparatus toward NADH was studied by evaluating the amperometric response to the addition of NADH and interferents (Fig 3 **Section f**). The substrate and product of the enzymatic reaction, the inhibitors tested and the solvent used for the inhibitor compounds are considered interferents. The electrochemical setup showed no interferences to the addition of these compounds while keeping a reliable current signal to the addition of NADH. It must be emphasized that NADH is a ubiquitous cofactor in cellular metabolism, and its direct electrochemical detection would inherently lack selectivity in complex biological fluids, where many NADH-dependent enzymes are active [104]. The present work, however, was not designed for direct application in such matrices, but rather as a starting point of the development of a biosensor for a cell-free, buffer-

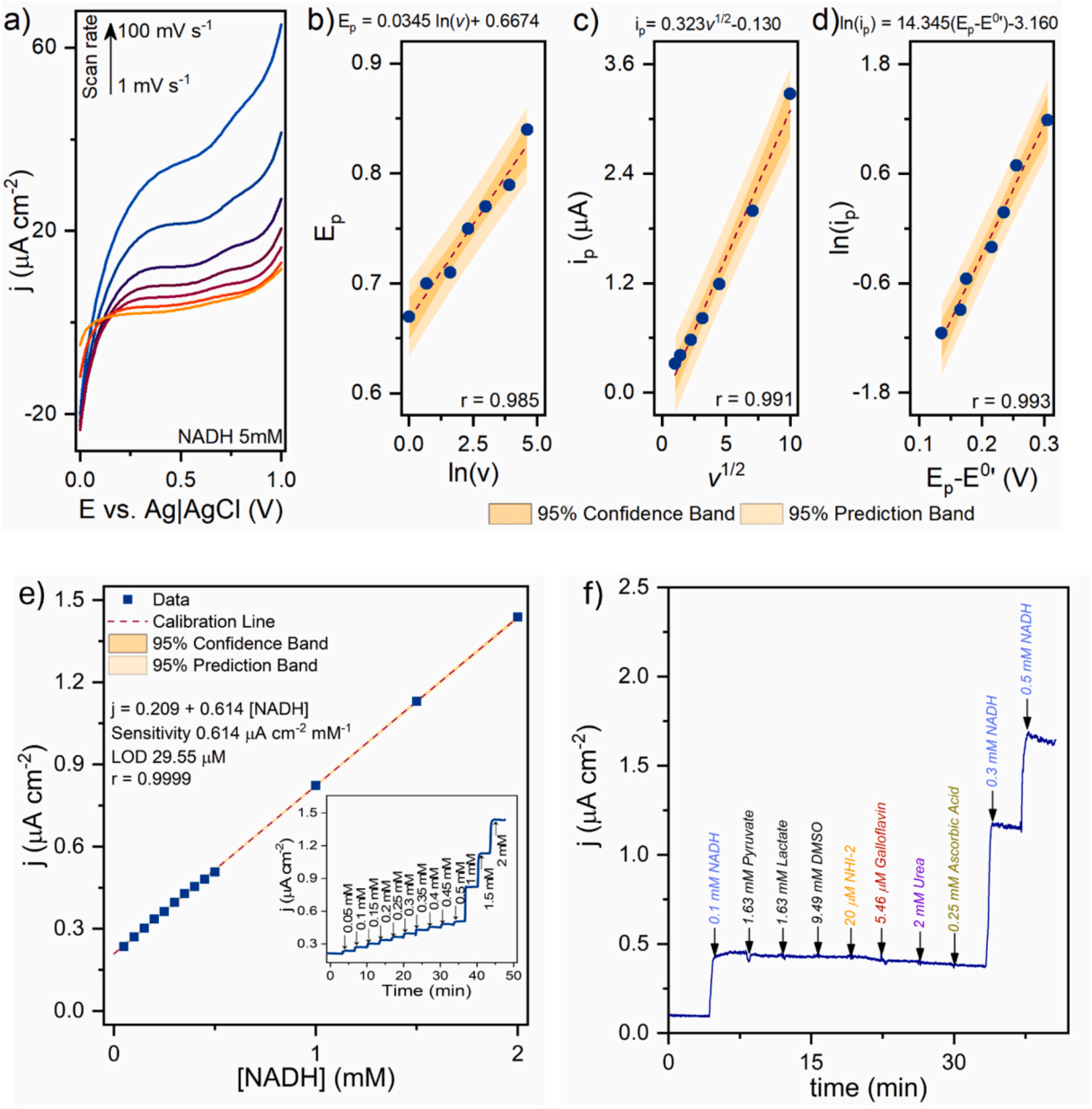


**Fig. 3.** Linear sweep voltammetric response of 5 mM NADH (phosphate buffer solution pH 7.5) at scan rates 1–100 mV s-1 (a). Variation of peak potential vs. logarithm of scan rate (b). Variation of peak current vs. square root of the scan rate (c). Variation of logarithm of peak current vs. peak potential (d). (e) Calibration curve of current density vs. NADH concentration. The insert shows the amperometric response with respect to the increase of NADH concentration and (f) amperometric response of the electrochemical system with respect to the addition of NADH and different compounds necessary for the enzymatic reaction (1.63 mM pyruvate, 1.63 mM lactate, 9.44 mM DMSO, 20 µM NHI-2, 5.46 µM galloflavin, 2 mM urea and 0.25 mM ascorbic acid).

based assay aimed at monitoring LDH activity and its inhibition. Within this controlled environment, NADH serves as an effective and reproducible reporter of enzymatic turnover, quite adequate for the intended purpose of inhibitor screening [105–107]. Nevertheless, potential interferents such as urea (2 mM) and ascorbic acid (0.25 mM), which are not expected to be present under the intended screening conditions, were also tested. Their lack of interference with the NADH current signal suggests, however, that the biosensor could potentially be applied in more complex environments than the controlled one envisaged for drug screening.

An additional robustness assessment of the electrode was performed by evaluating the inter-day reproducibility of the electrode response toward NADH. To evaluate the robustness of the electrode, a single Ti/Nafion-modified glassy carbon electrode was tested repeatedly over seven days in 0.1 M phosphate buffer (pH 7.5) containing 5 mM NADH. Each day, 15 consecutive CV cycles were recorded, and the anodic peak current was measured. At the end of each session, the electrode was rinsed with Milli-Q water for 10 min and subsequently stored at 4 °C in phosphate buffer until the next measurement day.

A slight, progressive increase in peak current was observed from day to day (**Fig. S16 section a**), which shows the first and the last CVs for each day. This drift can be attributed to electrochemical activation and hydration-induced structural rearrangements of the Nafion–Ti film. Such behavior is well documented for Nafion-coated electrodes during their initial use, where film swelling and ion uptake can alter the electroactive surface and charge transport properties before reaching a stable regime [108–110]. This phenomenon reflects surface stabilization rather than degradation.

Quantitatively, the inter-day RSD of the anodic peak current was 9.57 %, whereas the intra-day repeatability remained high. This level of

variability is fully consistent with that typically reported for manually drop-cast electrodes, where inter-day variations in the range of 5–15 % are commonly observed [111]. These results confirm that the sensor exhibits adequate robustness for repeated use, supporting its suitability for routine LDH inhibitor screening.

An additional verification of the reliability of the electrochemical method was performed by comparing the calibrations of NADH concentrations obtained for current density (Fig 3 **Section e**) and the UV–vis absorption (**Fig. S17** of the SI). Fig 4 represents the current density obtained for each NADH concentration (ranging from 0.05 to 0.4 mM) as a function of the absorbance measured at 340 nm.

The strong correlation obtained from the linear fitting ($r = 0.986$) confirms that intrinsic experimental errors did not impact NADH concentration measurements in either analytical method. These results demonstrate that both methods are effective for NADH quantification. However, the electrochemical approach offers advantages over the optical method. Despite its lower LOD, the electrochemical quantification exhibits higher sensitivity. Moreover, the amperometric quantification covers a broader NADH concentration range, whereas UV–vis absorbance saturates at concentrations above 0.4 mM (**Fig. S17** of the SI). Finally, the electrochemical system appears not affected by the interference from compounds such as Galloflavin, NHI-2 or lactate (Fig 3 **Section f**), ensuring a more reliable monitoring of the enzymatic reaction and inhibitors' efficacy.

### 3.5. Electrochemical enzymatic response

Finally, the electrochemical response corresponding to the variation of NADH concentration obtained during the enzymatic reaction was evaluated both for soluble and immobilized *h*LDH-A, with and without NHI-2 and Galloflavin (Fig. 5). The enzymatic reactions were also monitored using UV–vis spectroscopy, and the curves obtained from both methods are displayed in **Fig. S18**.

The effect of the inhibitors was evaluated by comparing the rate of NADH oxidation in the presence of inhibitory compounds (**Sections c-f**) to that observed in their absence (**Sections a** and **b**). Table 1 summarized the results obtained.

For *h*LDH-A, the rate of NADH oxidation observed with NHI-2 and Galloflavin corresponds to 92 % and 78 %, respectively, of the value obtained without inhibitors. These outcomes suggest that Galloflavin is a more effective inhibitor. These findings are consistent with the apparent kinetic parameters obtained from kinetic studies (**Table S3**). A possible explanation for this phenomenon may be related to the type of secondary bonds formed between the enzyme and inhibitors, as revealed by molecular modeling simulations (**Fig S8**).

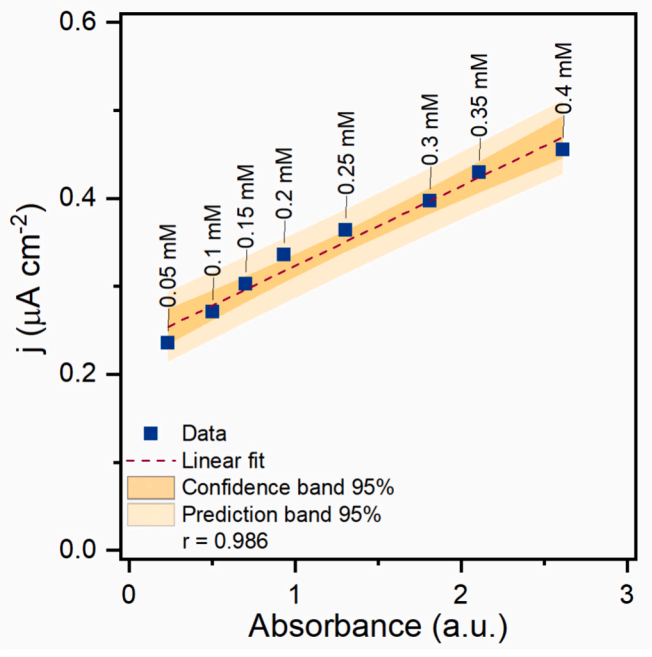


**Fig. 4.** Current density vs. UV–vis absorption at 340 nm for NADH concentration ranging from 0.05 to 0.4 mM.

The rates of NADH oxidation observed when the enzymatic reactions are catalyzed by the Biocat NHI-2 and Galloflavin correspond to 95 % and 69 %, respectively, of the value obtained without inhibitors. These findings aligned with the results achieved for *h*LDH-A. However, the signal is more disturbed, likely due to the lower activity of the enzyme in its immobilized form.

Several studies have shown that the overpotential for NADH oxidation can be markedly reduced (0.0–0.2 V) using nanostructured carbons, metallic nanoparticles, conducting polymers, or redox mediators [99,104,112–115]. These strategies achieve excellent sensitivity but typically involve more complex fabrication and higher costs. By contrast, the Ti-modified GCE employed here offers a simple and robust platform that provides stable NADH signals and accurate monitoring of LDH activity under controlled buffer conditions. While the working potential is higher, it does not compromise the present application.

A similar evaluation of the rate of NADH oxidation was conducted for the enzymatic reactions monitored using UV–vis spectroscopy. **Table S4** (SI) presents the results. It can be observed that when the optical method is used, the results of the free LDH and immobilized LDH are not comparable to each other or with the findings of amperometric measurements. Additionally, when the immobilized LDH catalyzes the reaction in the presence of NHI-2, it appears that a higher quantity of NADH is converted than is present. These discrepancies may be due to the absorption bands at 340 nm associated to NHI-2 and Galloflavin, which interfere with NADH signal **Fig S11**.

## 4. Conclusions

This study evaluates an electrochemical method as promising alternative to traditional UV–Vis spectroscopy for monitoring the enzymatic activity of human Lactate Dehydrogenase (*h*LDH-A), with particular focus on assessing inhibitory effects of potential anticancer drugs (NHI-2 and Galloflavin). The developed electrochemical system, based on a Ti-modified glassy carbon electrode, provided reliable amperometric quantification of NADH with high sensitivity (0.614 μA $cm^{-2}$ $mM^{-1}$), suitable selectivity, and negligible interference from reaction components and inhibitors. Chronoamperometric analyses effectively monitored enzymatic reactions catalyzed by both free and immobilized *h*LDH-A, clearly distinguishing inhibitory effects. The electrochemical method yielded consistent and reproducible results, demonstrating that Galloflavin exhibits stronger inhibition compared to NHI-2 for both free and immobilized enzyme forms. These findings were supported by molecular docking analyses, indicating that Galloflavin's more effective inhibition likely results from specific hydrogen-bond interactions. On the other hand, UV–Vis spectroscopic analysis faced limitations due to spectral interferences caused by possible absorption bands of inhibitors, leading to unreliable or non-comparable results. Particularly, NHI-2 significantly interfered with NADH detection at 340 nm. Overall, the electrochemical approach may exhibit several advantages over the optical method, providing accurate, interference-resistant, robust and sensitive measurements suitable for real-time monitoring of LDH inhibition. The proposed electrochemical sensor offers a well-balanced compromise between simplicity, cost-effectiveness and analytical performance. However, combining both UV–Vis spectroscopy and electrochemical methods could provide a more robust analytical strategy, minimizing the risk of false positives and false negatives.

This makes the proposed electrochemical setup particularly promising for rapid screening of anticancer drug candidates targeting metabolic pathways mediated by LDH enzymes.

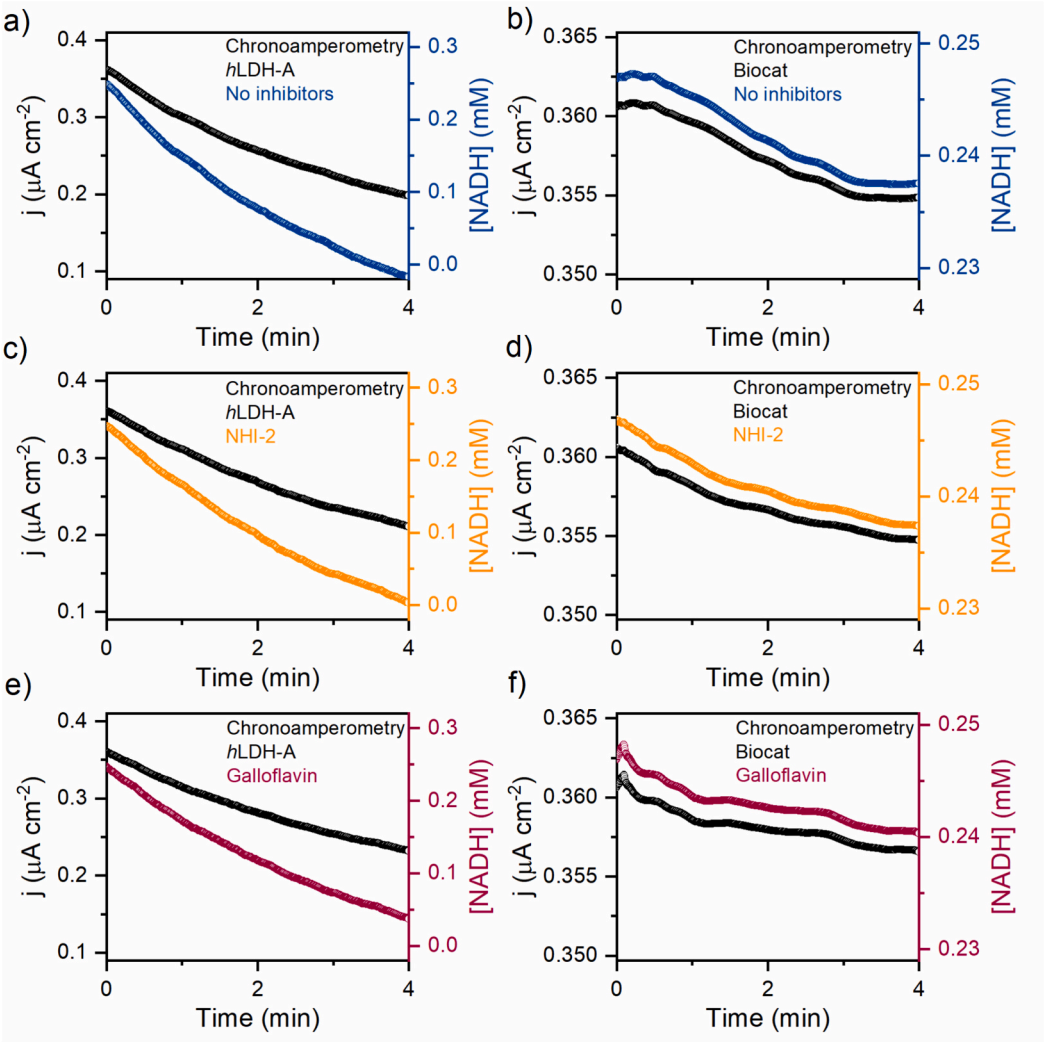


**Fig. 5.** Amperometric response at 0.66 V of the pyruvate reduction catalyzed by lactate dehydrogenase (a), (c), (e) in its soluble (*h*LDH-A) and (b), (d), (f) immobilized (Biocat) forms. The reaction was studied without inhibitors and with NHI-2 (20 μM) or galloflavin (5.64 μM).

**Table 1**
Rate of NADH oxidation obtained by enzymatic reaction catalyzed by the soluble and immobilized *h*LDH-A without and with inhibitors monitored with chronoamperometric measurements. Results are expressed as moles of NADH oxidized per minute (μmol $min^{-1}$).

| | No inhibitors | NHI-2 | Galloflavin |
|---|---|---|---|
| *h*LDH-A | 1.04 ± 0.95 | 0.95 ± 0.88 | 0.81 ± 0.75 |
| Biocat | 0.08 ± 0.009 | 0.07 ± 0.004 | 0.05 ± 0.003 |

## CRediT authorship contribution statement

**Chiara Vincenzi:** Writing – review & editing, Writing – original draft, Investigation. **Clarissa Cocuzza:** Writing – review & editing, Writing – original draft, Investigation, Formal analysis, Data curation, Conceptualization. **Andrés Illanes:** Writing – review & editing. **Debora Fino:** Funding acquisition. **Simelys Hernández:** Writing – review & editing, Supervision, Methodology. **Valentina Cauda:** Writing – review & editing, Investigation. **Carminna Ottone:** Writing – review & editing, Supervision, Methodology, Formal analysis. **Marco Piumetti:** Writing – review & editing, Supervision, Project administration.

## Funding sources

No competing financial interests have been declared.

## Declaration of competing interest

The authors declare that they have no known competing financial interests or personal relationships that could have appeared to influence the work reported in this paper.

## Appendix A. Supplementary data

Supplementary data to this article can be found online at https://doi.org/10.1016/j.microc.2025.115963.

## Data availability

Data will be made available on request.

## References

[1] I.A. for R. on C, IARC, Globocan 2022 (2022). https://gco.iarc.who.int (accessed October 1, 2024).
[2] J. Gan, W. Wang, Z. Yang, J. Pan, L. Zheng, L. Yin, Prognostic value of pretreatment serum lactate dehydrogenase level in pancreatic cancer patients A

meta-analysis of 18 observational studies, Medicine (United States) 97 (2018), https://doi.org/10.1097/MD.0000000000013151.
[3] G. Varma, P. Seth, P. Coutinho de Souza, C. Callahan, J. Pinto, M. Vaidya, O. Sonzogni, V. Sukhatme, G.M. Wulf, A.K. Grant, Visualizing the effects of lactate dehydrogenase (LDH) inhibition and LDH-A genetic ablation in breast and lung cancer with hyperpolarized pyruvate NMR, NMR Biomed. 34 (2021), https://doi.org/10.1002/nbm.4560.
[4] Y. Wei, H. Xu, J. Dai, J. Peng, W. Wang, L. Xia, F. Zhou, Prognostic significance of serum lactic acid, lactate dehydrogenase, and albumin levels in patients with metastatic colorectal Cancer, Biomed. Res. Int. 2018 (2018), https://doi.org/10.1155/2018/1804086.
[5] B. Cui, Y. Luo, P. Tian, F. Peng, J. Lu, Y. Yang, Q. Su, B. Liu, J. Yu, X. Luo, L. Yin, W. Cheng, F. An, B. He, D. Liang, S. Wu, P. Chu, L. Song, X. Liu, H. Luo, J. Xu, Y. Pan, Y. Wang, D. Li, P. Huang, Q. Yang, L. Zhang, B.P. Zhou, S. Liu, G. Xu, E.W. F. Lam, K.W. Kelley, Q. Liu, Stress-induced epinephrine enhances lactate dehydrogenase A and promotes breast cancer stem-like cells, J. Clin. Investig. 129 (2019) 1030–1046, https://doi.org/10.1172/JCI121685.
[6] L. Sun, J. Li, W. Yan, Z. Yao, R. Wang, X. Zhou, H. Wu, G. Zhang, T. Shi, W. Chen, H19 promotes aerobic glycolysis, proliferation, and immune escape of gastric cancer cells through the microRNA-519d-3p/lactate dehydrogenase A axis, Cancer Sci. 112 (2021) 2245–2259, https://doi.org/10.1111/cas.14896.
[7] F. Cascardo, N. Anselmino, A. Páez, E. Labanca, P. Sanchis, V. Antico-Arciuch, N. Navone, G. Gueron, E. Vázquez, J. Cotignola, Ho-1 modulates aerobic glycolysis through ldh in prostate cancer cells, Antioxidants 10 (2021), https://doi.org/10.3390/antiox10060966.
[8] S.L. Zhang, Y. He, K.Y. Tam, Targeting cancer metabolism to develop human lactate dehydrogenase (hLDH)5 inhibitors, Drug Discov. Today 23 (2018) 1407–1415, https://doi.org/10.1016/j.drudis.2018.05.014.
[9] U. Aday, A. Böyük, H. Akkoç, The prognostic significance of serum lactate dehydrogenase-to-albumin ratio in colorectal cancer, Ann Surg Treat Res 99 (2020) 161–170, https://doi.org/10.4174/astr.2020.99.3.161.
[10] A. Tjokrowidjaja, S.J. Lord, T. John, C.R. Lewis, P.S. Kok, I.C. Marschner, C. K. Lee, Pre- and on-treatment lactate dehydrogenase as a prognostic and predictive biomarker in advanced non–small cell lung cancer, Cancer 128 (2022) 1574–1583, https://doi.org/10.1002/cncr.34113.
[11] Y. Kobayashi, K. Banno, H. Kunitomi, T. Takahashi, T. Takeda, K. Nakamura, K. Tsuji, E. Tominaga, D. Aoki, Warburg effect in Gynecologic cancers, J. Obstet. Gynaecol. Res. 45 (2019) 542–548, https://doi.org/10.1111/jog.13867.
[12] S. Daniele, C. Giacomelli, E. Zappelli, C. Granchi, M.L. Trincavelli, F. Minutolo, C. Martini, Lactate dehydrogenase-A inhibition induces human glioblastoma multiforme stem cell differentiation and death, Sci. Rep. 5 (2015) 1–17, https://doi.org/10.1038/srep15556.
[13] R. Kusumawati, A.H. Nasrullah, R.N. Pesik, D. Indarto Muthmainah, Secondary Metabolites of *Mirabilis jalapa* Structurally Inhibit Lactate Dehydrogenase A In Silico: A Potential cancer Treatment, IOP Conf Ser Mater Sci Eng, Institute of Physics Publishing, in, 2018, https://doi.org/10.1088/1757-899X/333/1/012078.
[14] K. Augoff, A. Hryniewicz-Jankowska, R. Tabola, Lactate dehydrogenase 5: An old friend and a new hope in the war on cancer, Cancer Lett. 358 (2015) 1–7, https://doi.org/10.1016/j.canlet.2014.12.035.
[15] J.K. Byun, Tumor lactic acid: a potential target for cancer therapy, Arch. Pharm. Res. 46 (2023) 90–110, https://doi.org/10.1007/s12272-023-01431-8.
[16] A. Comandatore, M. Franczak, R.T. Smolenski, L. Morelli, G.J. Peters, E. Giovannetti, Lactate dehydrogenase and its clinical significance in pancreatic and thoracic cancers, Semin. Cancer Biol. 86 (2022) 93–100, https://doi.org/10.1016/j.semcancer.2022.09.001.
[17] W. Xing, X. Li, Y. Zhou, M. Li, M. Zhu, Lactate metabolic pathway regulates tumor cell metastasis and its use as a new therapeutic target, Explor Med 4 (2023) 541–549, https://doi.org/10.37349/emed.2023.00160.
[18] U. Aluru, A. Patel, A. Rogers, S. Lalani, M. Nafea, S. Godwin-Offor, A. Bullock, A. Shankar, E. Tadvai, J. Boccucci, G.G. Raval, Baseline LDH as a prognostic biomarker of early treatment failure in lung cancer, J. Clin. Oncol. 43 (2025), https://doi.org/10.1200/JCO.2025.43.16_suppl.e20023.
[19] J. Chen, X. Zou, Prognostic significance of lactate dehydrogenase and its impact on the outcomes of gastric cancer: a systematic review and meta-analysis, Front. Oncol. 13 (2023), https://doi.org/10.3389/fonc.2023.1247444.
[20] Y. Zhou, M. Qi, M. Yang, Current status and future perspectives of lactate dehydrogenase detection and medical implications: A review, Biosensors (Basel) 12 (2022) 1145, https://doi.org/10.3390/bios12121145.
[21] J. Shao, J. Feng, J. Li, S. Liang, W. Li, C. Wang, Novel tools for early diagnosis and precision treatment based on artificial intelligence, Chinese Medical Journal Pulmonary and Critical Care Medicine 1 (2023) 148–160, https://doi.org/10.1016/j.pccm.2023.05.001.
[22] D. Crosby, S. Bhatia, K.M. Brindle, L.M. Coussens, C. Dive, M. Emberton, S. Esener, R.C. Fitzgerald, S.S. Gambhir, P. Kuhn, T.R. Rebbeck, S. Balasubramanian, Early Detection of cancer, Science (1979) 375, 2022, https://doi.org/10.1126/science.aay9040.
[23] J. Xiang, L. Zhou, Y. He, S. Wu, LDH-A inhibitors as remedies to enhance the anticancer effects of PARP inhibitors in ovarian cancer cells, Aging 13 (2021) 25920–25930, https://doi.org/10.18632/aging.203780.
[24] E. Varghese, S.M. Samuel, A. Líšková, M. Samec, P. Kubatka, D. Büsselberg, Targeting glucose metabolism to overcome resistance to anticancer chemotherapy in breast Cancer, Cancers (Basel) 12 (2020) 2252, https://doi.org/10.3390/cancers12082252.
[25] M. Wang, Q. Zhou, T. Cao, F. Li, X. Li, M. Zhang, Y. Zhou, Lactate dehydrogenase A: a potential new target for tumor drug resistance intervention, J. Transl. Med. 23 (2025) 713, https://doi.org/10.1186/s12967-025-06773-z.
[26] U.S. Food and Drug administration, The Drug Development Process, in: https://www.fda.gov/patients/learn-about-drug-and-device-approvals/drug-development-process, 2018 accessed October 1, 2024.
[27] L. Wang, Y. Song, H. Wang, X. Zhang, M. Wang, J. He, S. Li, L. Zhang, K. Li, L. Cao, Advances of artificial intelligence in anti-Cancer drug design: A review of the past decade, Pharmaceuticals 16 (2023), https://doi.org/10.3390/ph16020253.
[28] W. Cui, A. Aouidate, S. Wang, Q. Yu, Y. Li, S. Yuan, Discovering anti-Cancer drugs via computational methods, Front. Pharmacol. 11 (2020) 1–14, https://doi.org/10.3389/fphar.2020.00733.
[29] S. Arana-Peña, D. Carballares, R. Morellon-Sterling, J. Rocha-Martin, R. Fernandez-Lafuente, The combination of covalent and ionic exchange immobilizations enables the coimmobilization on vinyl sulfone activated supports and the reuse of the most stable immobilized enzyme, Int. J. Biol. Macromol. 199 (2022) 51–60, https://doi.org/10.1016/j.ijbiomac.2021.12.148.
[30] O. Barbosa, R. Torres, C. Ortiz, Á. Berenguer-Murcia, R.C. Rodrigues, R. Fernandez-Lafuente, Heterofunctional supports in enzyme immobilization: from traditional immobilization protocols to opportunities in tuning enzyme properties, Biomacromolecules 14 (2013) 2433–2462, https://doi.org/10.1021/bm400762h.
[31] X.-C. Zhang, L. Hou, H. Cai, J.-M. Zhang, F.-Z. Chen, J. Peng, W.-W. Zhao, Synergetic Enzyme-Incorporated Metal–Organic Framework and Polyoxometalate Nanozyme: Achieving Stable Tandem Catalysis for Organic Photoelectrochemical Transistor Bioanalysis, Anal. Chem. 96 (2024) 16355–16361, https://doi.org/10.1021/acs.analchem.4c03786.
[32] Y. Liu, W. Xu, W. Zhuge, Q. Huang, G. Xiang, J. Peng, Conductive aluminum phthalocyanine-based porous organic polymer as an efficient electrocatalyst for nifedipine detection, Sens Actuators B Chem 404 (2024) 135191, https://doi.org/10.1016/j.snb.2023.135191.
[33] C. Zhang, W. Ou, Z. Zeng, H. Liu, K. Yu, L. Wang, L. Zhou, Polypyrrole participates in the construction of a polarity-switchable photoelectrochemical molecularly imprinted sensor for the detection of acrylamide in fried foods, Sens Actuators B Chem 402 (2024) 135037, https://doi.org/10.1016/j.snb.2023.135037.
[34] S. Tvorynska, J. Barek, B. Josypcuk, High-performance amperometric biosensor for flow injection analysis consisting of a replaceable lactate oxidase-based mini-reactor and a silver amalgam screen-printed electrode, Electrochim. Acta 445 (2023), https://doi.org/10.1016/j.electacta.2023.142033.
[35] R.L.F. Melo, F.S. Neto, D.N. Dari, B.C.C. Fernandes, T.M. Freire, P.B.A. Fechine, J. M. Soares, J.C.S. dos Santos, A comprehensive review on enzyme-based biosensors: advanced analysis and emerging applications in nanomaterial-enzyme linkage, Int. J. Biol. Macromol. 264 (2024), https://doi.org/10.1016/j.ijbiomac.2024.130817.
[36] O. Josypčuk, J. Barek, B. Josypčuk, Electrochemical biosensors based on enzymatic reactors filled by various types of silica and amalgam powders for measurements in flow systems, Electroanalysis 28 (2016) 3028–3038, https://doi.org/10.1002/elan.201600273.
[37] S. Tvorynska, J. Barek, B. Josypčuk, Flow amperometric uric acid biosensors based on different enzymatic mini-reactors: A comparative study of uricase immobilization, Sens Actuators B Chem 344 (2021), https://doi.org/10.1016/j.snb.2021.130252.
[38] S. Tvorynska, J. Barek, B. Josypčuk, Amperometric biosensor based on enzymatic reactor for choline determination in flow systems, Electroanalysis 31 (2019) 1901–1912, https://doi.org/10.1002/elan.201900237.
[39] P. Bollella, Enzyme-based amperometric biosensors: 60 years later … quo Vadis? Anal. Chim. Acta 1234 (2022) 340517 https://doi.org/10.1016/j.aca.2022.340517.
[40] N. Carlsson, H. Gustafsson, C. Thörn, L. Olsson, K. Holmberg, B. Åkerman, Enzymes immobilized in mesoporous silica: A physical-chemical perspective, Adv. Colloid Interface Sci. 205 (2014) 339–360, https://doi.org/10.1016/j.cis.2013.08.010.
[41] D. Alagöz, A. Toprak, N.E. Varan, D. Yildirim, S.S. Tükel, Effective immobilization of lactate dehydrogenase onto mesoporous silica, Biotechnol. Appl. Biochem. (2021) 1–11, https://doi.org/10.1002/bab.2304.
[42] D. Gößl, H. Singer, H.Y. Chiu, A. Schmidt, M. Lichtnecker, H. Engelke, T. Bein, Highly active enzymes immobilized in large pore colloidal mesoporous silica nanoparticles, New J. Chem. 43 (2019) 1671–1680, https://doi.org/10.1039/c8nj04585b.
[43] C. Bernal, L. Sierra, M. Mesa, Improvement of thermal stability of β-galactosidase from *Bacillus circulans* by multipoint covalent immobilization in hierarchical macro-mesoporous silica, J. Mol. Catal. B: Enzym. 84 (2012) 166–172, https://doi.org/10.1016/j.molcatb.2012.05.023.
[44] G. Pietricola, T. Tommasi, M. Dosa, E. Camelin, E. Berruto, C. Ottone, D. Fino, V. Cauda, M. Piumetti, Synthesis and characterization of ordered mesoporous silicas for the immobilization of formate dehydrogenase (FDH), Int. J. Biol. Macromol. 177 (2021) 261–270, https://doi.org/10.1016/j.ijbiomac.2021.02.114.
[45] S. Hudson, J. Cooney, E. Magner, Proteins in mesoporous silicates, Angewandte Chemie - International Edition 47 (2008) 8582–8594, https://doi.org/10.1002/anie.200705238.
[46] Y. Zhao, Q. Hu, F. Cheng, N. Su, A. Wang, Y. Zou, H. Hu, X. Chen, H.-M. Zhou, X. Huang, K. Yang, Q. Zhu, X. Wang, J. Yi, L. Zhu, X. Qian, L. Chen, Y. Tang, J. Loscalzo, Y. Yang, SoNar, a highly responsive NAD+/NADH sensor, allows

high-throughput metabolic screening of anti-tumor agents, Cell Metab. 21 (2015) 777–789, https://doi.org/10.1016/j.cmet.2015.04.009.
[47] S. Deng, X. Men, M. Hu, X. Liang, Y. Dai, Z. Zhan, Z. Huang, H. Chen, Z. Dong, Ratiometric fluorescence sensing NADH using AIE-dots transducers at the point of care, Biosens. Bioelectron. 250 (2024) 116082, https://doi.org/10.1016/j.bios.2024.116082.
[48] J. Lee, H.N. Suh, S. Ahn, H. Bin Park, J.Y. Lee, H.J. Kim, S.H. Kim, Disposable electrocatalytic sensor for whole blood NADH monitoring, Sci. Rep. 12 (2022) 16716, https://doi.org/10.1038/s41598-022-20995-x.
[49] E.V. Potapova, E.A. Zherebtsov, V.V. Shupletsov, V.V. Dremin, K.Y. Kandurova, A.V. Mamoshin, A.Y. Abramov, A.V. Dunaev, Detection of <scp>NADH</scp> and <scp>NADPH</scp> levels *in vivo* identifies shift of glucose metabolism in cancer to energy production, FEBS J. 291 (2024) 2674–2682, https://doi.org/10.1111/febs.17067.
[50] A.M. Baracu, L.A. Dinu Gugoasa, Review—recent advances in microfabrication, design and applications of Amperometric sensors and biosensors, J. Electrochem. Soc. 168 (2021) 037503, https://doi.org/10.1149/1945-7111/abe8b6.
[51] P. Bollella, L. Gorton, Enzyme based amperometric biosensors, Curr Opin, Electrochem 10 (2018) 157–173, https://doi.org/10.1016/j.coelec.2018.06.003.
[52] F. Otero, T. Mandal, D. Leech, E. Magner, An electrochemical NADH biosensor based on a nanoporous gold electrode modified with diaphorase and an osmium polymer, Sensors and Actuators Reports 4 (2022), https://doi.org/10.1016/j.snr.2022.100117.
[53] L. Meng, A.P.F. Turner, W.C. Mak, Positively-charged hierarchical PEDOT interface with enhanced electrode kinetics for NADH-based biosensors, Biosens. Bioelectron. 120 (2018) 115–121, https://doi.org/10.1016/j.bios.2018.08.017.
[54] C.H. Chen, Y.C. Chen, M.S. Lin, Amperometric determination of NADH with Co3O4 nanosheet modified electrode, Biosens. Bioelectron. 42 (2013) 379–384, https://doi.org/10.1016/j.bios.2012.10.086.
[55] S.B. Prasanna, A.A.A. Bahajjaj, Y.H. Lee, Y.C. Lin, U. Dhawan, R. Sakthivel, R. J. Chung, Highly responsive and sensitive non-enzymatic electrochemical sensor for the detection of β-NADH in food, environmental and biological samples using AuNP on polydopamine/titanium carbide composite, Food Chem. 426 (2023) 136609, https://doi.org/10.1016/j.foodchem.2023.136609.
[56] C. Cocuzza, C. Vincenzi, C. Ottone, A. Illanes, D. Fino, V. Cauda, M. Piumetti, Synthesis and characterization of mesoporous silicas with dendritic and spongy-like structures : potential supports for human lactate dehydrogenase-based microreactors aimed at anticancer inhibitor screening, Microporous Mesoporous Mater. 376 (2024) 113182, https://doi.org/10.1016/j.micromeso.2024.113182.
[57] C. Cocuzza, G. Pietricola, I. Zonca, M. Dosa, O. Romero, T. Tommasi, V. Cauda, D. Fino, C. Ottone, M. Piumetti, Simultaneous CO 2 reduction and NADH regeneration using formate and glycerol dehydrogenase enzymes co-immobilized on modified natural zeolite, RSC Adv. 12 (2022) 31142–31155, https://doi.org/10.1039/d2ra03459j.
[58] C. Cocuzza, E. Antoniono, C. Ottone, V. Cauda, D. Fino, M. Piumetti, Preparation of a mesoporous biosensor for lactate dehydrogenase (hLDH-A) as potential anticancer inhibitor screening, ACS Biomater Sci. Eng. 9 (2023) 6045–6057, https://doi.org/10.1021/acsbiomaterials.3c00582.
[59] H.P. Erickson, Size and shape of protein molecules at the nanometer level determined by sedimentation, gel filtration, and electron microscopy, Biol Proced Online 11 (2009) 32–51, https://doi.org/10.1007/s12575-009-9008-x.
[60] J. Rocha-Martín, B. de Las Rivas, R. Muñoz, J.M. Guisán, F. López-Gallego, Rational co-immobilization of bi-enzyme cascades on porous supports and their applications in bio-redox reactions with insitu recycling of soluble cofactors, ChemCatChem 4 (2012) 1279–1288, https://doi.org/10.1002/cctc.201200146.
[61] S. Kim, J. Chen, T. Cheng, A. Gindulyte, J. He, S. He, Q. Li, B.A. Shoemaker, P.A. Thiessen, B. Yu, L. Zaslavsky, J. Zhang, E.E. Bolton, PubChem 2023 update, Nucleic Acids Res. 51 (2023) D1373–D1380. Doi:https://doi.org/10.1093/nar/gkac956.
[62] A. Sobczak, T. Rebiś, G. Milczarek, Electrocatalysis of NADH oxidation using electrochemically activated fluphenazine on carbon nanotube electrode, Bioelectrochemistry 106 (2015) 308–315, https://doi.org/10.1016/j.bioelechem.2015.07.002.
[63] H. Hamidi, B. Haghighi, Fabrication of a sensitive amperometric sensor for NADH and H2O2 using palladium nanoparticles-multiwalled carbon nanotube nanohybrid, Mater. Sci. Eng. C 62 (2016) 423–428, https://doi.org/10.1016/j.msec.2016.01.058.
[64] L.V. da Silva, C.B. Lopes, W.C. da Silva, Y.G. de Paiva, F. de A. dos S. Silva, P. R. Lima, L.T. Kubota, M.O.F. Goulart, Electropolymerization of ferulic acid on multi-walled carbon nanotubes modified glassy carbon electrode as a versatile platform for NADH, dopamine and epinephrine separate detection, Microchem. J. 133 (2017) 460–467, https://doi.org/10.1016/j.microc.2017.04.014.
[65] E. Sharifi, A. Salimi, E. Shams, Electrocatalytic activity of nickel oxide nanoparticles as mediatorless system for NADH and ethanol sensing at physiological pH solution, Biosens. Bioelectron. 45 (2013) 260–266, https://doi.org/10.1016/j.bios.2013.01.055.
[66] J. Zhu, X. Chen, W. Yang, A high performance electrochemical sensor for NADH based on graphite nanosheet modified electrode, Sens Actuators B Chem 150 (2010) 564–568, https://doi.org/10.1016/j.snb.2010.08.039.
[67] R. Rajaram, S. Anandhakumar, J. Mathiyarasu, Electrocatalytic oxidation of NADH at low overpotential using nanoporous poly(3,4)-ethylenedioxythiophene modified glassy carbon electrode, J. Electroanal. Chem. 746 (2015) 75–81, https://doi.org/10.1016/j.jelechem.2015.03.028.
[68] M.M. Rahman, M.M. Alam, A.M. Asiri, S. Chowdhury, R.S. Alruwais, Sensitive detection of citric acid in real samples based on Nafion/ZnO–CuO nanocomposites modified glassy carbon electrode by electrochemical approach, Mater. Chem. Phys. 293 (2023) 126975, https://doi.org/10.1016/j.matchemphys.2022.126975.
[69] G. Li, S. Feng, L. Yan, L. Yang, B. Huo, L. Wang, S. Luo, D. Yang, Direct electrochemical detection of cu(II) ions in juice and tea beverage samples using MWCNTs-BMIMPF6-Nafion modified GCE electrodes, Food Chem. 404 (2023), https://doi.org/10.1016/j.foodchem.2022.134609.
[70] H. Alwael, S.H. Al-Sedran, M. Oubaha, N.A.A. Asiri, A.S. Bashammakh, A. S. Alharthy, N.A. Albassami, T.N. Abduljabbar, G.I. Mohammed, H.M. Nassef, E. A. Bahaidarah, B.G. Alhogbi, M.S. El-Shahawi, Probe –integrated electrochemical sensing platform for measuring trace levels of parathion pesticides residues in water using au- nanoparticles anchored Nafion nano composite modified glassy carbon electrode, J. Food Compos. Anal. 124 (2023) 105649, https://doi.org/10.1016/j.jfca.2023.105649.
[71] K.Y. Tsai, H.F. Peng, J.J. Huang, Nafion modified electrochemical sensor integrated with a feedback-loop indium-gallium-zinc oxide thin-film transistor for enhancing dopamine detection limit, Sens Actuators A Phys 354 (2023) 114287, https://doi.org/10.1016/j.sna.2023.114287.
[72] B. Zhou, N. Qi, B. Wang, Z.Q. Chen, Effect of swelling agent on the pore structure of SBA-15 studied by positron annihilation, Appl. Surf. Sci. 475 (2019) 961–968, https://doi.org/10.1016/j.apsusc.2019.01.056.
[73] M. Piumetti, B. Bonelli, P. Massiani, S. Dzwigaj, I. Rossetti, S. Casale, L. Gaberova, M. Armandi, E. Garrone, Effect of vanadium dispersion and support properties on the catalytic activity of V-SBA-15 and V-MCF mesoporous materials prepared by direct synthesis, Catal. Today 176 (2011) 458–464, https://doi.org/10.1016/j.cattod.2010.10.066.
[74] M. Piumetti, B. Bonelli, P. Massiani, Y. Millot, S. Dzwigaj, L. Gaberova, M. Armandi, E. Garrone, Novel vanadium-containing mesocellular foams (V-MCF) obtained by direct synthesis, Microporous and Mesoporous Materials 142 (2011) 45–54, https://doi.org/10.1016/j.micromeso.2010.11.010.
[75] Z. Chen, F.C. Hsu, D. Battigelli, H.C. Chang, Capture and release of viruses using amino-functionalized silica particles, Anal. Chim. Acta 569 (2006) 76–82, https://doi.org/10.1016/j.aca.2006.03.103.
[76] N.I. Sabeela, T.M. Almutairi, H.A. Al-Lohedan, A.O. Ezzat, A.M. Atta, Reactive mesoporous ph-sensitive amino-functionalized silica nanoparticles for efficient removal of coomassie blue dye, Nanomaterials 9 (2019), https://doi.org/10.3390/nano9121721.
[77] J.O. Otalvaro, M. Avena, M. Brigante, Adsorption of organic pollutants by amine functionalized mesoporous silica in aqueous solution, Effects of pH, ionic strength and some consequences of APTES stability, J Environ Chem Eng 7 (2019) 103325, https://doi.org/10.1016/j.jece.2019.103325.
[78] M.C. Ruiz-Cañas, L.M. Corredor, H.I. Quintero, E. Manrique, A.R. Romero Bohórquez, Morphological and structural properties of amino-functionalized fumed nanosilica and its comparison with nanoparticles obtained by modified Stöber method, Molecules 25 (2020), https://doi.org/10.3390/molecules25122868.
[79] M. Thommes, K.A. Cychosz, Physical adsorption characterization of nanoporous materials: Progress and challenges, Adsorption 20 (2014) 233–250, https://doi.org/10.1007/s10450-014-9606-z.
[80] M. Thommes, K. Kaneko, A.V. Neimark, J.P. Olivier, F. Rodriguez-Reinoso, J. Rouquerol, K.S.W. Sing, Physisorption of gases, with special reference to the evaluation of surface area and pore size distribution (IUPAC technical report), Pure Appl. Chem. 87 (2015) 1051–1069, https://doi.org/10.1515/pac-2014-1117.
[81] M. Carbonaro, A. Nucara, Secondary structure of food proteins by Fourier transform spectroscopy in the mid-infrared region, Amino Acids 38 (2010) 679–690, https://doi.org/10.1007/s00726-009-0274-3.
[82] K. Bouchmella, Q. Lion, C. Gervais, M.B. Cardoso, Impact of mesoporous silica functionalization fine-tuning on antibiotic uptake/delivery and bactericidal activity, ACS Omega 8 (2023) 12154–12164, https://doi.org/10.1021/acsomega.2c08065.
[83] M. Hiraoui, M. Guendouz, N. Lorrain, A. Moadhen, L. Haji, M. Oueslati, Spectroscopy studies of functionalized oxidized porous silicon surface for biosensing applications, Mater. Chem. Phys. 128 (2011) 151–156, https://doi.org/10.1016/j.matchemphys.2011.02.052.
[84] J.M. Guisan, J.M. Bolivar, F. López-Gallego, J. Rocha-Martín (Eds.), Immobilization of Enzymes and Cells Methods and Protocols, 4th ed., Humana Press, Hatfield, Hertfordshire, UK, 2020.
[85] M. Piumetti, A. Illanes, Enzymes and Their Function, in: Molecular Dynamics and Complexity in Catalysis and Biocatalysis, Springer International Publishing, 2022, pp. 23–53, https://doi.org/10.1007/978-3-030-88500-7_2.
[86] A. Illanes, C. Altamirano, L. Wilson, in: A. Illanes (Ed.), Homogeneous Enzyme Kinetics BT - Enzyme Biocatalysis: Principles and Applications, Springer, Netherlands, Dordrecht, 2008, pp. 107–153, https://doi.org/10.1007/978-1-4020-8361-7_3.
[87] R.D. Crapnell, A. Garcia-Miranda Ferrari, N.C. Dempsey, C.E. Banks, Electroanalytical overview: screen-printed electrochemical sensing platforms for the detection of vital cardiac, cancer and inflammatory biomarkers, Sensors & Diagnostics 1 (2022) 405–428, https://doi.org/10.1039/D1SD00041A.
[88] A.S. Lorenzetti, T. Sierra, C.E. Domini, A.G. Lista, A.G. Crevillen, A. Escarpa, Electrochemically reduced graphene oxide-based screen-printed electrodes for Total tetracycline determination by adsorptive transfer stripping differential pulse voltammetry, Sensors 20 (2019) 76, https://doi.org/10.3390/s20010076.
[89] S.A. Spring, S. Goggins, C.G. Frost, Ratiometric electrochemistry: improving the robustness, reproducibility and reliability of biosensors, Molecules 26 (2021) 2130, https://doi.org/10.3390/molecules26082130.

[90] B. Zhang, L. Wang, S.-J. Chang, Y. Jing, T. Sun, Z. Lei, C.-J. Chen, J.-T. Liu, Flexible cellulose paper-based biosensor from inkjet printing for non-invasive glucose monitoring, Polym. Test. 137 (2024) 108527, https://doi.org/10.1016/j.polymertesting.2024.108527.
[91] Z. Dai, G. Lu, J. Bao, X. Huang, H. Ju, Low potential detection of NADH at titanium-containing MCM-41 modified glassy carbon electrode, Electroanalysis 19 (2007) 604–607, https://doi.org/10.1002/elan.200603769.
[92] M. Elancheziyan, K. Theyagarajan, V.K. Ponnusamy, K. Thenmozhi, S. Senthilkumar, Porous graphene oxide based disposable non-enzymatic electrochemical sensor for the determination of nicotinamide adenine dinucleotide, Micro and Nano Engineering 15 (2022) 100133, https://doi.org/10.1016/j.mne.2022.100133.
[93] A.C. Lazanas, M.I. Prodromidis, Electrochemical Impedance Spectroscopy—A Tutorial, ACS Measurement Science Au 3 (2023) 162–193, https://doi.org/10.1021/acsmeasuresciau.2c00070.
[94] A. Lasia, Electrochemical Impedance Spectroscopy and its Applications, Springer New York, New York, NY, 2014, https://doi.org/10.1007/978-1-4614-8933-7.
[95] C.M.A. Brett, Electrochemical impedance spectroscopy in the characterisation and application of modified electrodes for electrochemical sensors and biosensors, Molecules 27 (2022) 1497, https://doi.org/10.3390/molecules27051497.
[96] E. Boselli, Z. Wu, E.N. Haynes, I. Papautsky, Screen-printed sensors modified with Nafion and mesoporous carbon for electrochemical detection of Lead in blood, J. Electrochem. Soc. 171 (2024) 027513, https://doi.org/10.1149/1945-7111/ad2397.
[97] F. Zhou, Y. Yan, S. Guan, W. Guo, M. Sun, M. Pan, Solving Nafion poisoning of <scp>ORR</scp> catalysts with an accessible layer: designing a nanostructured core-shell Pt/C catalyst via a one-step self-assembly for <scp>PEMFC</scp>, Int. J. Energy Res. 44 (2020) 10155–10167, https://doi.org/10.1002/er.5629.
[98] J.M. Mazurków, A. Kusior, M. Radecka, Electrochemical characterization of modified glassy carbon electrodes for non-enzymatic glucose sensors, Sensors 21 (2021) 7928, https://doi.org/10.3390/s21237928.
[99] S. Immanuel, R. Sivasubramanian, Electrochemical studies of NADH oxidation on chemically reduced graphene oxide nanosheets modified glassy carbon electrode, Mater. Chem. Phys. 249 (2020) 123015, https://doi.org/10.1016/j.matchemphys.2020.123015.
[100] H. Wang, S.Y. Sayed, E.J. Luber, B.C. Olsen, S.M. Shirurkar, S. Venkatakrishnan, U.M. Tefashe, A.K. Farquhar, E.S. Smotkin, R.L. McCreery, J.M. Buriak, Redox flow batteries: how to determine electrochemical kinetic parameters, ACS Nano 14 (2020) 2575–2584, https://doi.org/10.1021/acsnano.0c01281.
[101] R. Guidelli, R.G. Compton, J.M. Feliu, E. Gileadi, J. Lipkowski, W. Schmickler, S. Trasatti, Defining the transfer coefficient in electrochemistry: An assessment (IUPAC technical report), Pure Appl. Chem. 86 (2014) 245–258, https://doi.org/10.1515/pac-2014-5026.
[102] M.G. Trachioti, A.C. Lazanas, M.I. Prodromidis, Shedding light on the calculation of electrode electroactive area and heterogeneous electron transfer rate constants at graphite screen-printed electrodes, Microchim. Acta 190 (2023) 1–14, https://doi.org/10.1007/s00604-023-05832-w.
[103] N. Delmo, B. Mostafiz, A.E. Ross, J. Suni, E. Peltola, Developing an electrochemical sensor for the in vivo measurements of dopamine, Sensors and Diagnostics 2 (2023) 559–581, https://doi.org/10.1039/d2sd00230b.
[104] X. Jin, M. Zhong, Z. Zhu, J. Xie, J. Feng, Y. Liu, J. Guo, B. Li, J. Liu, Application of NAD+-dependent electrochemical dehydrogenase biosensors in human physiological fluids: opportunities and challenges, J. Anal. Methods Chem. 2023 (2023) 1–13, https://doi.org/10.1155/2023/3401001.
[105] D. Annas, S.-Y. Cheon, M. Yusuf, S.-J. Bae, K.-T. Ha, K.H. Park, Synthesis and initial screening of lactate dehydrogenase inhibitor activity of 1,3-benzodioxole derivatives, Sci. Rep. 10 (2020) 19889, https://doi.org/10.1038/s41598-020-77056-4.
[106] S. Shibata, S. Sogabe, M. Miwa, T. Fujimoto, N. Takakura, A. Naotsuka, S. Kitamura, T. Kawamoto, T. Soga, Identification of the first highly selective inhibitor of human lactate dehydrogenase B, Sci. Rep. 11 (2021) 21353, https://doi.org/10.1038/s41598-021-00820-7.
[107] E.-Y. Kim, T.-W. Chung, C.W. Han, S.Y. Park, K.H. Park, S.B. Jang, K.-T. Ha, A novel lactate dehydrogenase inhibitor, 1-(Phenylseleno)-4-(trifluoromethyl) benzene, Suppresses Tumor Growth through Apoptotic Cell Death, Sci Rep 9 (2019) 3969, https://doi.org/10.1038/s41598-019-40617-3.
[108] S.P. Shylendra, M. Wajrak, K. Alameh, J.J. Kang, Nafion modified titanium nitride pH sensor for future biomedical applications, Sensors 23 (2023) 699, https://doi.org/10.3390/s23020699.
[109] A. Kelarakis, Nafion in biomedicine and healthcare, Polymers (Basel) 17 (2025) 2054, https://doi.org/10.3390/polym17152054.
[110] A.F. Claire, P. Zacher, D. Lehto, D. Krahn, K.L. Knoche Gupta, Electrochemical characterization of recast Nafion® film-modified electrodes in acetonitrile with various electrolytes, Electrochem 5 (2024) 574–584, https://doi.org/10.3390/electrochem5040037.
[111] J. Wang, Analytical Electrochemistry, 3rd ed., Wiley-VCH, 2006.
[112] L. Zhu, J. Zhai, R. Yang, C. Tian, L. Guo, Electrocatalytic oxidation of NADH with Meldola's blue functionalized carbon nanotubes electrodes, Biosens. Bioelectron. 22 (2007) 2768–2773, https://doi.org/10.1016/j.bios.2006.12.027.
[113] Y. Fan, Y. Liu, G. Gao, H. Zhang, J. Zhi, Development and application of an electrochemical sensor with 1,10-Phenanthroline-5,6-dione-modified electrode for the detection of Escherichia coli in water, Chemosensors 11 (2023) 458, https://doi.org/10.3390/chemosensors11080458.
[114] R.H. de Oliveira, D.A. Gonçalves, D.D. dos Reis, TiO2/MWCNT/Nafion-modified glassy carbon electrode as a sensitive Voltammetric sensor for the determination of hydrogen peroxide, Sensors 23 (2023) 7732, https://doi.org/10.3390/s23187732.
[115] Z. Lucio-Rivera, G. Sanchez, W. Gorski, Amperometric determination of NADH and dehydrogenase enzymes at a redox-active nanocomposite, Talanta 286 (2025) 127434, https://doi.org/10.1016/j.talanta.2024.127434.